FARADAY

Electron spin echo modulation study of the Type I copper protein rusticyanin and its mutant variant His85Ala

Implications for the general analysis of weak ^{14}N superhyperfine interactions

Christopher J. Bender,[a]* Danilo R. Casimiro,[b]† Jack Peisach[a] and H. Jane Dyson[b]

[a] *Department of Molecular Pharmacology, Albert Einstein College of Medicine, 1300 Morris Park Avenue, Bronx, NY 10461, USA*

[b] *Department of Molecular Biology, The Scripps Research Institute, 10666 North Torrey Pines Road, La Jolla, CA 92037, USA*

Electron spin echo modulation (ESEEM) spectra were recorded at 500 MHz intervals for the Type I protein rusticyanin and its engineered variant His85Ala, which lacks one of the two imidazole ligands to copper. The Zeeman and g-value dependence of the spectral peaks were systematically mapped and accurately predicted that low intensity lines in the wild type (w.t.) spectrum were combination lines, as verified in the His85Ala spectra. Analysis reveals that the w.t. ESEEM spectra are attributable to a pair of $HisN_\varepsilon$ only, and the NQI parameters e^2Qq and η are 1.37 ± 0.03 MHz and 0.90 ± 0.05 for both $HisN_\varepsilon$ in the w.t. protein. The nuclear hyperfine interaction is estimated as 1.8 MHz, and includes a dipolar interaction of 0.5 MHz. The principal difference between the two imidazole nitrogen couplings is manifest in the dispersion of the combination lines, which suggests non-equivalent orientations of the respective superhyperfine tensors (or tilt of the imidazole ring). The protocol demonstrates a general procedure for accurately determining superhyperfine parameters from powder ESEEM spectra. Finally, peak shifts among ESEEM spectra of His85Ala—X (X = H_2O, Cl^-, Br^-) demonstrate that the imidazole ligand powder superhyperfine spectrum is sensitive to chemical effects in the metal's ligand sphere, thus suggesting that the method may be used for evaluation in molecular design.

1 Introduction

Rusticyanin is a Type I (blue) copper protein whose function and unique spectroscopic properties are similar to proteins of the same class, such as azurin and plastocyanin.[1] Rusticyanin, however, is unique because the prokaryotic organism from which it is isolated, *Thiobacillus ferrooxidans*, grows in highly acidic (pH 0–4) conditions.[2] The protein is therefore of interest from the standpoint of protein stability and integrity of the copper site in what is ordinarily considered a hostile environment. In this paper we report the electron spin echo modulation (ESEEM) spectra of weakly coupled ^{14}N nuclei located within the ligand sphere of copper in rusticyanin and test the hypothesis that the associated weak superhyperfine couplings are sensitive to local chemical effects by using an engineered form of the protein that binds exogenous ligands.

Our purpose in performing a detailed ESEEM spectroscopic study of rusticyanin is two-fold. Besides our interest in the unique structural stability of rusticyanin and whether this leads to unusual histidine side chain interactions, we are motivated by the protein engineering capabilities of modern molecular biology and wish to assess ESEEM spectroscopy as a means to detect small shifts in superhyperfine parameters that may accompany site-directed mutagenesis of a metal binding site. Typical powder ESEEM spectra of paramagnetic copper–imidazole complexes feature very narrow lines that occur at frequencies very close to the theoretical zero-field nuclear quadrupole resonance transition frequencies of the tri-coordinate $>N-H$ fragment of imidazole, which suggests that the ESEEM method might be used to determine nuclear quadrupole interaction (NQI) parameters, namely e^2Qq, and the asymmetry parameter η, to high accuracy despite the inhomogeneously broadened spectral lines of the frozen solution sample. The significance of this spectroscopic capability resides with the relationship between the NQI parameters and the chemical factors, such as orbital hybridization and molecular structure.[3]

Rusticyanin possesses the characteristic Type I copper binding motif $CysHis_2Met$,[4] and in the case of rusticyanin, three of these ligands, Cys138, His143 and Met148, were identified by homology with the C-terminal sequences of other blue copper proteins of this class.[5–7] Although EXAFS showed that the ligand set was most likely standard and contained a histidine as the fourth ligand,[8,9] the identity of this ligand was uncertain, in part, because of the extremely low sequence homology between rusticyanin and other proteins. The fourth ligand was conclusively identified as His85 by NMR,[10] site-directed mutagenesis of His85 to Ala,[11] and three-dimensional structures of the protein by NMR[12,13] (reduced Cu^I form) and X-ray crystallography[14] (oxidized Cu^{II} form). A representation of the copper coordination sphere is shown in Fig. 1.

ESEEM spectroscopy[15] provides a useful tool for probing the weakly interacting nuclei in the sphere of metal complexes. The electron spin echo amplitude is measured as a function of the interpulse spacing, and the resultant time series generates an interferogram[16] of the precession frequencies corresponding to those nuclei coupled to the electron spin. In general, the method is best suited to low-frequency nuclear precessions, and the classic electron spin echo study of copper imidazole complexes has demonstrated that the deep echo modulation is attributable to the non-bonding nitrogen atom of the imidazole ring, for which the magnitude of the nuclear quadrupole interaction, the nuclear Zeeman interaction, and the nuclear hyperfine interaction are all approximately equal.[17] The

† Present address: Department of Human Genetics, Merck Research Laboratories, Rahway, NJ 07065, USA

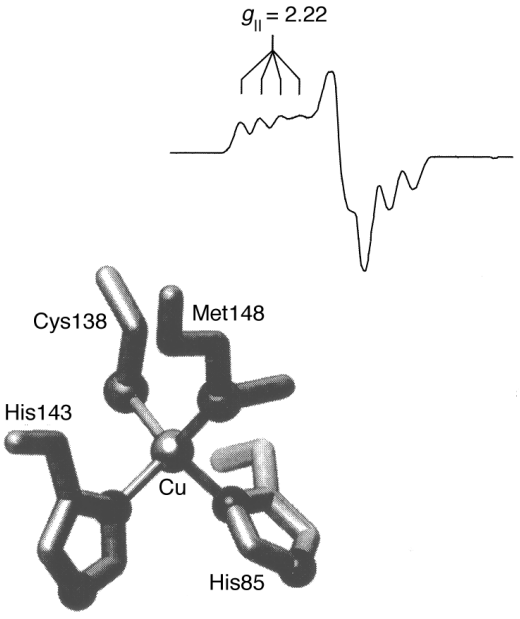

Fig. 1 Structure and continuous-wave EPR spectrum of w.t. rusticyanin. The spectrum was recorded at 77 K, 9.5 GHz, 2 mW incident microwave power, and 2 G_{pp} field modulation. The His85Ala mutant lacks one histidine ligand to copper, yet the EPR spectrum is identical. The structure is drawn from ref. 13.

Fourier transform spectrum of the echo modulation time series contains intense lines that very nearly correspond to the effective zero-field nuclear quadrupole transition frequencies of the free imidazole >N—H fragment, which is attributed to the effective cancellation of the nuclear Zeeman and hyperfine energies in one m_S spin manifold.[17]

As applied to the Type I copper center, ESEEM is therefore sensitive to the superhyperfine interaction of the non-bonding nitrogen atom of the histidine imidazole side chains (*i.e.* $HisN_\varepsilon$). Only two spectral lines are necessary to determine the nuclear quadrupole parameters e^2Qq and η of ^{14}N fully, and it is therefore possible, in principle, to characterize fully NQI parameters that, in turn, may be used to infer chemical and structural information.[3] Our ESEEM study of the native and single imidazole forms of rusticyanin is, in part, intended as an examination of quantitative assignments of NQI parameters that are based upon the spectra near 'exact cancellation'. On the basis of the Zeeman-dependent behavior of the powder ESEEM spectral features[18] we outline an experimental protocol for greatly improving the accuracy of assigning the ESEEM spectral lines to specific transitions within the spin manifold and thereby deriving numerical parameters.

The availability of His85Ala rusticyanin and its ability to bind exogenous anions also enabled us to examine the echo modulation phenomenon in detail not afforded by many model compounds or metalloproteins and to test ESEEM spectroscopy of powder samples as an analytical technique in molecular design. For example, the modulation behavior of a single imidazole nitrogen and its variation under the effect of 'g-selection' is facilitated by the deletion of one histidine ligand to copper in the mutant protein that retains its characteristics. The deletion of one histidine ligand also removes the mechanism that generates so-called 'combination' lines that arise when two or more equivalent nuclei interact with the electron spin. Their absence in the mutant His85Ala will potentially unmask any contributions that might arise from weak (peptide) nitrogen superhyperfine interactions. Finally, His85Ala binds exogenous anions, which occupy the vacancy left by the removal of His85, and therefore provides us with a sample with which to test whether small shifts in the ESEEM spectrum can be observed in response to chemical effects.

2 Experimental

2.1 Description of the spectrometer

The ability to measure the Zeeman dependence of the ESEEM spectral lines is a key element to their assignment and quantitative interpretation. The home-built pulsed EPR spectrometer that was used in this study is made operable over three octaves by broadband components. Microwave pulses of 15 ns duration are generated at low power by gating a continuous wave synthesized microwave source (Gigatronics 905; 2–20 GHz). The output of the synthesizer (+15 dBm max) is passed to the reference arm and receiver (LO input), but a portion of this signal is sampled by using a directional coupler and amplified (Hewlett-Packard 8348A; +24 dBm, 2–20 GHz) prior to insertion into a two-channel pulse forming circuit. Each channel consists of two 20 dB isolators spanned by a fast switch, an attenuator, and an adjustable line.[19] The low-power pulses are then passed to a traveling wave tube so that each amplified 15 ns pulse delivers 25 W of microwave power when operated with no attenuation. The pulses are not strictly $90°$–τ–$90°$–t–$90°$ in the stimulated echo data collection sequence; three pulses of equal length are generated and the (pulse amplitude) power is raised until the maximum echo amplitude is achieved. The validity of operating under these conditions has been described.[16,20] The 15 ns pulses saturate an approximately 18 G portion of the EPR spectral envelope; no ESEEM spectral resolution enhancement was detected by switching to 40 ns pulse widths.

Echo detection is made *via* a homodyne receiver, and phase cycling is employed to eliminate spurious echoes that arise from the three-pulse sequence. The receiver front end consists of a PIN diode limiter, gating switch, and a low noise GaAs FET amplifier. The LO input of the double balanced mixer is supplied with approximately +10 dBm continuous wave power and isolated from the transmitter portion of the spectrometer. The video output of the mixer is amplified in stages by one or more high-bandwidth amplifiers. The echo is sampled by a gated integrator that features a 16 ns aperture and linear response to an input range 0–1 V. The amplifier output is adjusted so that the output signal is approximately 0.4 V at the mid-range of the echo modulation time series. This ensures that the echo amplitude remains within the linear range of the gated integrator for all points in the time series while retaining the optimum dynamic range.

A transmission mode sample resonator[21] was used. Each resonator is a brass block into which is formed an H-shaped well that is approximately 1 in deep. The shaped block serves as a shunt for two parallel waveguide transmission lines and it is therefore an octave device. A $\lambda/2$ rectangular strip resides in the bridge between the two shunted lines and electrically couples the two lines. The structure behaves as a low-Q transmission line bandpass filter (pass band $f_C \pm 32$ MHz) whose center frequency is set by the strip's length, and discrete operating frequencies for experiments can be obtained by preparing a set of strips. In the X-band region, for example, typical strip dimensions are 0.0313 in × 0.1875 in × l, where $0.330 < l/\text{in} < 0.420$.

The spectrometer configuration requires only a change of the traveling wave tube, ferrite components, and the waveguide probehead when switching between octaves.

2.2 Sample preparation for spectroscopy

The His85Ala and wild type (w.t.) protein were prepared as described previously[10–13] and received for spectroscopy at a protein concentration of 1.8 mM in 10 mM H_2SO_4 (pH 3.8). All samples were diluted 1 : 1 with chilled ethylene glycol and immediately loaded into the sample resonator. The pH of the glass forming sample mixture was verified against standard

pHydrion (Brooklyn, NY) indicator paper. No difference in spectral peak position or relative intensity was observed when 'neat' (dilution with buffer) protein samples were compared to the glycol-containing sample solution; the improved glass formed by the latter improved the echo's symmetry.

2.3 Post-processing of the modulation time series

The experimental echo modulation time series decay monotonically due to spin–lattice relaxation and loss of phase memory (spin coherence). This decay is approximately exponential and affects the quality of the Fourier transform spectrum by skewing the baseline at low frequency and relative line intensities in the spectrum. A six-point spline was used to reproduce this decay functionally and to correct the experimental data. This processing of the data sufficed for time series obtained with a combined τ plus starting t of approximately 200–300 ns; longer times (*i.e.* operation with large τ) required reconstruction of the 'lost' modulation, and the windowing method of Mims[22] was applied. The simulation methods that are used to test assigned hyperfine parameters create discrete cosine FT spectra by using the same algorithms and numerical routines.

3 Assignment of the ESEEM spectral lines

3.1 Identification of the echo modulation frequencies

The stimulated echo modulation time series of w.t. rusticyanin was recorded at 500 MHz intervals over the entire X-band (7–13 GHz) operating range of the probehead. Select Fourier transform spectra are cataloged in Fig. 2 according to spectrometer operating frequency and g-value, and each spectrum contains characteristic features that can be assigned on the basis of their magnetic field dependence. In each of the spectra shown, the three-pulse echo modulation was recorded with a τ value that corresponds to twice the period of the proton Larmor precession (*i.e.* $2\omega_H^{-1}$; typically $120 \leqslant \tau \leqslant 170$ ns). The replicate experiments, which are used to compile a 'catalog' of characteristic ESEEM modulation frequencies and their Zeeman field dependence, were conducted in such a manner as to maintain specific orientations of the magnetic parameters relative to the molecular reference frame (*i.e.* 'g-selection' of hyperfine and quadrupole tensoral elements).

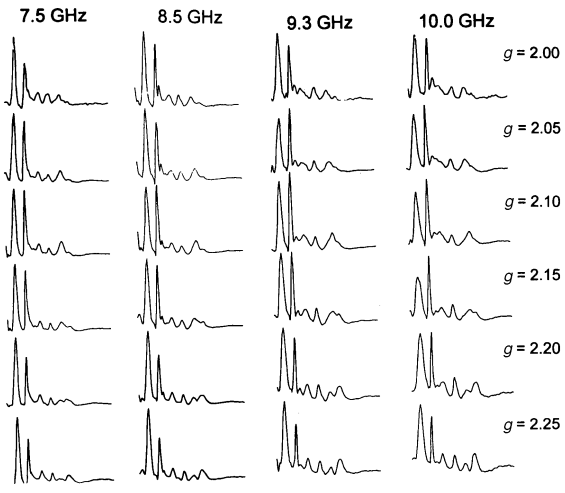

Fig. 2 Stimulated echo modulation spectra (0–6 MHz) of w.t. rusticyanin recorded over the EPR spectral envelope (discrete g-values) and at several spectrometer operating frequencies across the 8–12 GHz octave. The spectra are similar with respect to their shape, which reflects the pattern described for weak ^{14}N couplings at exact cancellation (ref. 17), yet the Zeeman field dependence is evident as measurable shifts in peak position and lineshape, plots of which are used to graphically analyze and assign spin Hamiltonian parameters. The temporal spacing between pulses 1 and 2 is fixed at twice the Larmor precession period of the proton, approximately 150 ns at the operating frequencies indicated.

At these low τ values, the echo modulation time series (see Fig. 3) can be decomposed by observation into three principal components. The initial 1 μs of the time series reveals a relatively shallow oscillation with period of approximately 250 ns ($f \approx 4$ MHz). The longest-lived and dominant component of the modulation has a period of *ca.* 650 ns and corresponds to the intense and narrow peak that is observed at 1.5 MHz in the FT spectrum. The third component is less obvious, but appears as an asymmetric repeating pattern (much more evident in modulation series in which the 1.5 MHz line is suppressed, see subsequent sections and Fig. 6) that resembles a rectified sinusoidal wave and has a period of *ca.* 1.4 s ($f \approx 700$ kHz). These three components correspond to the three principal spectroscopic features that are observed in the ESEEM superhyperfine spectrum.

Minor, less intense, spectral lines appear in the w.t. spectrum both among the two low-frequency peaks and in the region between 2 and 4 MHz. As will be discussed further below, these weak lines can be attributed to any of a variety of possible electron–nuclear interactions or combination/sum lines of the two intense peaks centered at 0.7 and 1.5 MHz. As a first step towards determining the origin of the low-intensity peaks, the time domain data are subjected to a deconvolution and reconstruction procedure. Fig. 3 illustrates two representative modulation time series (recorded at 9.0 GHz) and their deconvolution into component frequencies by the Mims windowing method.[22] The experimental data (time series as top

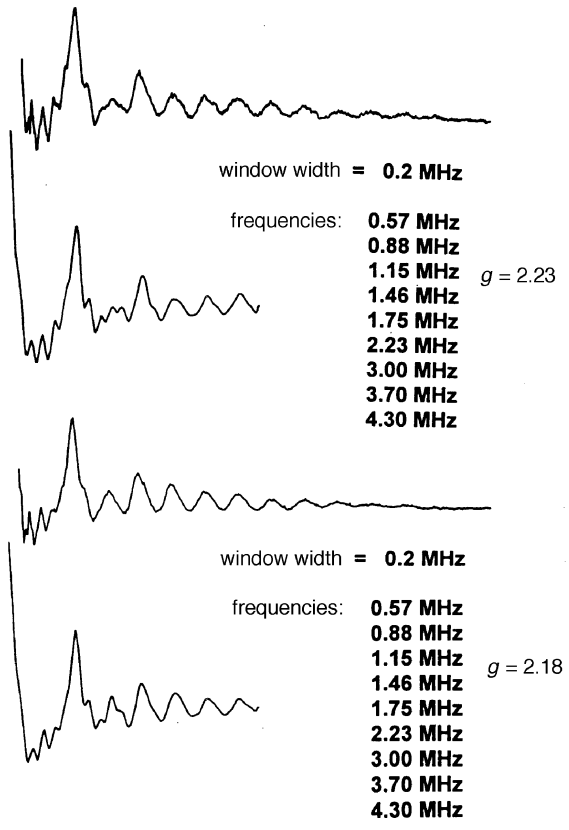

Fig. 3 Representative echo modulation time series and reconstruction by applying the Mims windowing method (ref. 22). Raw data (top trace) are windowed with the width and frequencies indicated. The reconstruction are derived from the listed frequencies and weighted by the amplitudes of the peaks observed in the FT spectrum. The excellent fidelity of the reconstructed time series indicates that our analysis and identification of the modulation components from the FT spectrum is correct (*i.e.* there are no missing or obscured peaks).

trace of each pair) are compared to a reconstruction that was generated by the indicated window width and frequencies, and the fidelity of reproduction is excellent.

The frequencies that are used in the windowing procedure and listed alongside the data correspond to features observed in the FT spectrum, and they are readily assigned within the context of the six-level ENDOR energy diagram for $I = 1$ nuclear hyperfine interaction. The broad feature centered at 0.7 MHz (see Fig. 2) is assumed to be a doublet of closely spaced peaks each having a linewidth comparable to the sharp peak at 1.5 MHz. This assumption follows from the original interpretation of copper–imidazole ESEEM[17] and corroborated by our *g*-selection experiments with the single imidazole interaction ESEEM of His85Ala, which demonstrate splitting of the 0.7 MHz feature (Section 3.5).

The spectra depicted in Fig. 2 reveal weak features at frequencies 1.15 and 1.75 MHz, and these correspond to harmonics of the overlapping 0.57 and 0.88 MHz lines that are centered at 0.7 MHz. Our data therefore provide two means of resolving the frequencies of the apparently two overlapping lines. The first is *g*-selection, which splits the peaks in the single imidazole mutant (Section 3.5) and distorts the 0.7 MHz line in the w.t. spectra (Fig. 2). The second method of recognizing overlapping lines is *via* the sum and harmonic lines that appear when two or more equivalent nuclei are present and whose positions reflect the fundamentals according to simple rules. For example, the peak at 1.46 MHz in the w.t. spectrum is a sum frequency of the 0.57 and 0.88 MHz lines, but its much higher intensity (relative to the 1.15 and 1.75 MHz harmonics) suggests that it is a fundamental modulation frequency corresponding to a true ENDOR transition. Sums of 0.57 and 0.88 MHz with the 1.46 MHz line yield 2.23 and 2.34 MHz, and twice the 1.46 MHz line yields a harmonic of approximately 3 MHz. The 3.7 component appears to be a sum line of twice the 1.5 MHz frequency plus the 0.7 MHz components, whereas the 4.3 MHz component can not be correlated to any lower frequency line and interpreted as a fundamental frequency corresponding to a transition between nuclear sublevels; it is assigned to the so-called double quantum transition (ref. 17 and below). It would therefore appear that the two $HisN_\varepsilon$ are very nearly equivalent because there do not appear to be two independent sets of fundamental lines and harmonics, and each of the observable features in the rusticyanin ESEEM spectrum can be assigned on the basis of the simple imidazole model of Mims.[17] Selective enhancement and suppression of the individual components by varying τ was used to confirm the association of harmonic and sum lines with the fundamentals (see Section 3.3).

3.2 Assignment of the intense ESEEM lines

Fig. 4 illustrates a representative narrowed $g = 2.25$ spectrum (*i.e.* from Fig. 2) and summarizes the fundamental and major harmonic echo modulation frequencies described in the preceding paragraphs. The low-frequency peak near 700 kHz is regarded as a superposition of two lines (designated ν_{10} and ν_{1-} in accordance with a six-level energy level transition assignment; Fig. 4, inset) of width approximately the same as the intense line at 1.5 MHz (designated ν_{1+}), and it appears that the remaining lines are sums and harmonics of these three fundamental lines, as indicated in the figure. The three principal components of the echo modulation FT spectra, namely the broad 0.7 MHz feature, the narrow 1.5 MHz line and the 4 MHz feature, can be interpreted on the basis of previous studies of copper–imidazole complexes.[17,23–25] The two intense lines that appear at *ca.* 0.7 and 1.5 MHz are attributed to transitions among levels that are defined by an effective zero-field nuclear quadrupole interaction. In the perturbational expansion of the magnetic hyperfine interaction energy, $\mathcal{H} = \mathcal{H}_{NZ} + \mathcal{H}_{HF} + \mathcal{H}_Q$, the signs of the individual

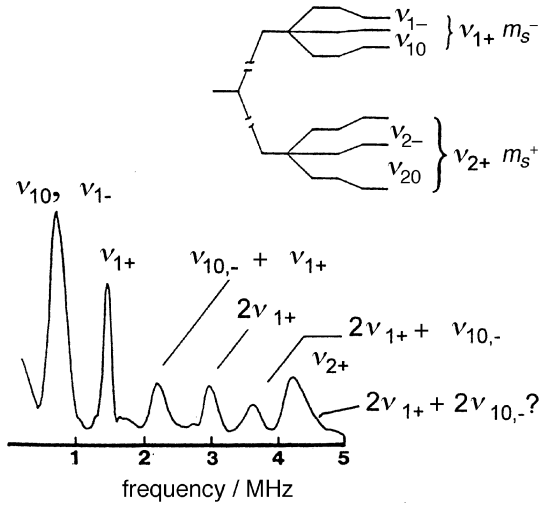

Fig. 4 A representative FT-spectrum of w.t. rusticyanin recorded at $g = 2.25$ and 9.0 GHz. The peaks in the 2–5 MHz range (compare with Fig. 2) have narrowed at $g = 2.25$, and their positions indicate that all lines in this region may be assigned to sums and harmonics of the effective zero-field NQR transitions, which are represented by the intense peaks below 2 MHz. The state diagram, based on the Mims model (ref. 17), and labeling used in the text are illustrated (inset).

energy terms depend on the sign of the product of m_S and m_I, and therefore $\mathcal{H}_{NZ}$ and $\mathcal{H}_{HF}$ add or subtract in opposing m_S spin manifolds (Fig. 4, inset).‡ When $\mathcal{H}_{NZ} = \mathcal{H}_{HF}$, the terms approximately cancel, leaving only $\mathcal{H}_Q$, and this simplistic description suffices for most ESEEM applications. Rigorously, however, the phenomenon resembles a crossing of energy levels in which the $I = -1$, 0, and $+1$ states mix, yielding cross-relaxation that enhances the modulation depth and spectral line intensity. The general perturbation theory[26] of near degenerate states predicts transition energies that are similar, but not identical, to those defined in Mims' simple model.[17]

The exact cancellation model[17,23–25] of interpreting ESEEM spectra is founded on the Townes–Daily model[27] of zero-field nuclear quadrupole interaction energies, and the intense low-frequency ESEEM transitions occur at frequencies approximated by $\nu_0 = \frac{1}{2}\eta e^2 Q q_{zz} h^{-1}$ and $\nu_\pm = \frac{3}{4}e^2 Q q_{zz}(1 \pm \frac{1}{3}\eta)h^{-1}$, where eq_{zz} is the *z*-axis component of the electric field gradient and η is a measure of the deviation of the electric field gradient tensor from axial symmetry ($0 \leqslant \eta \leqslant 1$).[27] The term eQ is the atomic nuclear quadrupole moment (approximately 9 MHz for a free nitrogen atom). Within this interpretative framework we assign the effective transition frequency ν_+ to the 1.5 MHz peak, ν_- to the 0.88 MHz peak, and ν_0 to the peak at 0.55 MHz (*i.e.* the frequencies determined by the back-transform fit depicted in Fig. 3). The justification for this assignment is further elaborated in subsequent sections citing the results of field dependence and τ suppression of the observed peaks.

The third principal contribution (*i.e.* modulation of period 250 ns) to the echo modulation corresponds to a broadened spectral line near 4 MHz and is assigned to a $\Delta m_I = 2$ transition in the m_S^+ spin manifold in which all the perturbational Hamiltonian terms add. This so-called 'double quantum' line varies with the magnitude of the dc magnetic field with a slope of $g_n\beta_n$, and it contains contributions from the nuclear Zeeman, nuclear hyperfine, and nuclear quadrupole inter-

‡ The terms m_S^+ and m_S^- will be used to denote the electronic spin states in which the nuclear Zeeman and hyperfine terms add and subtract, respectively, in the Mims description (ref. 17). Formally, the m_S^- state designation implies the set of nuclear sublevels that can be made to cross by manipulating H_0.

action terms.[17] This double quantum region near 4 MHz has been deconvoluted as two contributing features centered at 3.7 and 4.3 MHz because of the breadth and shape of the line, but as stated in the preceding paragraphs the 3.7 MHz contribution appears to be a sum line derived from the intense low-frequency lines, and not a second double quantum transition indicative of inequivalence of the two $HisN_{\varepsilon}$. Assignment of the 3.7 MHz line to a combination frequency (see following section) is made on the basis of its relative immobility as the Zeeman field is changed (the true double quantum transition at 4.0 MHz moves away from the 3.7 MHz line, see Fig. 2, $g = 2.25$ traces).

3.3 Assignment of weak ESEEM lines

The spectra of native rusticyanin, like many metal–imidazole complexes in protein, feature several lines in the region 2–4 MHz, and their origin could be one or more sources. As stated in the introduction, the copper atom is coordinated by two histidine imidazole side chains in the w.t. protein, and therefore we expect that the ESEEM spectrum will be a manifestation of electron–nuclear interactions from at least two remote imidazole nitrogen atoms, based upon ESEEM studies of copper–imidazole complexes.[17] The echo modulation contribution from two equivalent nuclei will lead to the observation of so-called 'combination lines' of the principal transition frequencies.[28] These combination lines are always observed when there are two or more equivalent nuclei interacting with the electron spin, and the phenomenon is analogous to the classical beat frequencies that are observed, for example, when two pendula are coupled. The frequencies predicted by this coupling are derived from the theory of linear mixing[29] and those specific to this study have been identified in a preceding section describing the results of a deconvolution and back transformation procedure.

A second source of transitions in this region, however, might be weakly coupled nitrogen atoms that are not associated with an imidazole side chain, such as amino nitrogen atoms of the peptide backbone that perhaps, for example, couple to the large spin density on the CysS *via* a hydrogen-bond bridge, or to the copper *via* spin delocalization from a primary ligand. The latter has been identified in ESEEM spectra of an azurin mutant His117Cys,[30] which, like the His85Ala rusticyanin mutant reported here, lacks one imidazole ligand to copper. Azurin features a fifth axial ligand, a Gly45 peptide carbonyl linkage to copper,[31] and a peak in the His117Cys azurin (reconstituted with [^{15}N]imidazole) ESEEM spectrum at approximately 2.8 MHz is assigned to the Gly45 amide nitrogen. Rusticyanin does not possess a fifth ligand at the axial position,[14] and therefore the weak lines that appear in the w.t. rusticyanin ESEEM spectrum cannot be attributed to such an interaction.

There is also the possibility that weak dipolar interactions between an amino nitrogen and the unpaired electron spin may occur *via* hydrogen bond interactions. For example, such amino nitrogen superhyperfine interactions have been suggested in the ESEEM spectrum of FeS centers in fumarate reductase, and the origin of this interaction is presumably a hydrogen-bond bridge between amino nitrogen atoms and cysteinyl sulfur atoms of the FeS cluster.[32] There are similar hydrogen bonds between the $Cys112S_{\gamma}$ of *Pseudomonas* azurin (based on X-ray structure and ^{15}N and ^{1}H NMR correlation spectra[33]), but the possibility of such an interaction being responsible for the weak 2–4 MHz peaks is precluded in the His85Ala ESEEM study (Section 3.5).

Finally, the β-protons of the ligand cysteine in Type I copper proteins are strongly coupled to the substantial spin density localized on $CysS_{\gamma}$, and the resultant proton hyperfine interactions will be large. ENDOR studies of other Type I proteins reveal that the $CysC_{\beta}$ protons typically have a hyperfine coupling constant of >20 MHz,[34,35] and, because the ENDOR transitions of these protons are paired according to the formula $\omega = \omega_{H} \pm \frac{1}{2}A$, it is possible that the low-frequency component of such a strongly coupled proton might reside in the region otherwise dominated by the weakly coupled nitrogen superhyperfine (shf) interactions.

Our experimental data preclude the assignment of any observed lines to a proton transition. The ESEEM spectra of rusticyanin were recorded over an extensive range of microwave (spectrometer operating) frequencies and corresponding magnetic fields, and under such conditions we would expect to observe shifts in proton lines commensurate with shifts in the nuclear Larmor frequency (ω_{i}) of the proton (see the formula in the preceding paragraph). None of the spectral lines observed in the rusticyanin ESEEM spectra (excluding the actual ^{1}H Larmor frequency that we do in fact observe) track as a function of the proton Larmor frequency, and therefore we conclude that no proton modulations are contributing to the low frequency spectral lines reported in this study.

3.4 The Zeeman dependence of ESEEM lines as an analytical tool

Although they are interpreted as zero-field values in the Townes–Daily context,[27] the lines attributed to the zero-field NQI transitions in the ESEEM spectrum do in fact shift as a function of the operating frequency/field and therefore data from spectra obtained at a single operating frequency cannot be used to compute e^2Qq and η unambiguously. The NQI fundamentals (most easily measured at the $\Delta m_I = 2$ transition that is designated as ν_+ and observed at approximately 1.5 MHz) shift by *ca.* 100 kHz GHz^{-1} in operating frequency, which corresponds to a Zeeman shift of *ca.* 400 Hz G^{-1}. At first this was believed to be due to a magnetic field dependent anticommutator (second-order term usually dropped in the spin-Hamiltonian), but prior analyses[18] suggest that the field-dependent behavior is primarily a consequence of the level-crossing process for the ^{14}N ($I = 1$) nuclear sublevels. At $g \geqslant 2.22$ the combination lines mirror the behavior of the fundamental lines, but are more difficult to track at g-values that represent a more diverse mixture of tensor orientations.

The ESEEM spectral behavior of the $S = \frac{1}{2}$, $I = 1$ system can be graphically depicted by plotting each transition frequency as a function of nuclear Zeeman energy. For all operating frequency/field combinations, that is, near and far from 'exact cancellation', the $\Delta m = 2$ transitions are the most intense of the set and are easiest to track as a field-dependent experimental observable. Weakly coupled nuclei, such as the remote imidazole nitrogen, are subjected to level-crossing conditions in the X-band region of spectrometer operating frequency, and the $\Delta m = 2$ transition frequency of the m_S sublevels undergoing crossing (Zeeman and hyperfine terms of opposite sign) will follow a parabolic trajectory through the level crossing condition. The opposite m_S spin manifold, in which the perturbation terms are additive, will not undergo nuclear sublevel crossings as H_0 is varied, and the trajectory of the corresponding $\Delta m = 2$ transition will be linear monotonic with increasing field strength, possibly leveling out at very low fields if the dipolar contribution to A is large. The $\Delta m = 2$ transitions associated with the m_S spin manifolds in which the nuclear hyperfine term adds or subtracts are designated ν_{2+} and ν_{1+} in this paper, respectively (see Fig. 4, inset).

Our data were recorded at frequencies ranging from 7 to 13 GHz, and the positions of the peaks were plotted as a function of the theoretically predicted ω_{N}. Table 1 lists the representative experimental data for the $\Delta m = 2$ transition frequencies, which are the most easy to resolve and to use as quantitative markers of the superhyperfine interaction. At the low-frequency limit of the operating range of the spectrometer, the

Table 1 Experimental frequencies of the $\Delta m = 2$ transitions (w.t. spectra) and the corresponding predicted frequencies based on the assigned shf parameters $e^2Qq = 1.35$ MHz, $\eta = 0.85$ and $A = 1.8$[a] MHz and a simple six-level energy diagram for ^{14}N ENDOR transitions[b]

		predicted		experimental	
frequency/GHz	ω_N/MHz	ν_{1+}/MHz	ν_{2+}/MHz	ν_{1+}/MHz	ν_{2+}/MHz
7.8	0.83	1.34	3.61	1.38	4.00
8.5	0.91	1.34	3.76	1.38	4.12
9.0	0.96	1.35	3.86	1.42	4.19
9.5	1.01	1.37	3.96	1.46	4.30
10.0	1.06	1.41	4.05	1.56	4.41

[a] Represents an upper estimate for a purely isotropic nuclear hyperfine coupling. [b] See L. Kevan and L. D. Kispert, *Electron Spin Double Resonance Spectroscopy*, Wiley, New York 1976, p. 185, Fig. 4–7. Note: The terminology used to describe the two $\Delta m = 2$ transitions in a six-level ENDOR energy diagram is illustrated in Fig. 4.

trajectory of the $\Delta m = 2$ line designated ν_{1+} had reached a constant value of 1.37 MHz, but not yet begun its upward trend with decreasing frequency/field (continuing to lower experimental operating frequency should shift ν_{1+} upwards, mirroring the trend observed at high frequency). In other words, the frequency minimum seems to have been reached and therefore indicates that the true point of exact cancellation is near 7.5 GHz ($H_0 = 2600$ G; $\omega_N = 0.80$ MHz). The double quantum line near 4 MHz, ν_{2+}, behaved as expected in a linear fashion and concurred with its assignment. Significantly, none of the peaks in the 2–4 MHz region behaved in a manner that would suggest that they were independent of the fundamental lines at 0.7 and 1.5 MHz; these peaks likewise reached a stationary lower limit and therefore must be harmonics of the quadrupole fundamentals. This observation is significant because if they were attributable to transitions of another set of nitrogen atoms of presumably different hyperfine coupling strength, then they would necessarily exhibit a field-dependent trajectory that differs from the imidazole nitrogen lines. None was observed, and we conclude that no nitrogen atoms other than those of the two HisN$_\varepsilon$ contribute to the observed ESEEM spectrum.

Table 1 also lists some predicted transition frequencies of the two $\Delta m = 2$ ENDOR transitions that are expected to be observed in an ESEEM experiment. The model that was used to calculate these frequencies is described in double resonance spectroscopy analyses[36] and follows from a six-level energy diagram and isotropic coupling terms. The parameters that are used to predict the transition frequencies, namely $e^2Qq = 1.4$ MHz, $\eta = 0.85$, and $A_{iso} = 1.7$ MHz, are crude approximates. The match to the experimental trend is good within 30%, but it must be remembered that the spectrum is a powder pattern and this crude approximation does not account for dipolar coupling nor for inhomogeneous line broadening. The simple model that was used here is merely intended as a starting point for further simulations that are described in Section 4. One striking aspect of these comparative data, however, is the observed shift in the $\Delta m = 2$ transition that is designated ν_{1+}, which is greater than would be predicted from the simple spin-Hamiltonian defined in the preceding section. This is tentatively being interpreted as evidence that the simple three-term spin-Hamiltonian model of ^{14}N ESEEM spectra[16] is inadequate. State mixing and second-order (anticommutator) Hamiltonian terms are being examined as probable causes of the disparity.

3.5 Echo modulation spectrum of the His85Ala protein

The ESEEM spectrum of the His85Ala protein is illustrated in Fig. 5 and underscores the interpretation of the w.t. spectrum. The conspicuous absence of lines in the 2–4 MHz region clearly demonstrates that a single imidazole is coordinated to copper, and furthermore, no lines are observed that could have been obscured by the combination lines in the w.t. spectra. The sharp feature that is located just to the high frequency side of the 1.5 MHz line in the w.t. spectrum (see especially Fig. 2, 9.8 GHz spectra) is also conspicuously absent, which illustrates that it too is a combination line. These data therefore illustrate that only the single remaining His143N$_\varepsilon$ contributes to the His85Ala ESEEM spectrum. Identical plots of the linear electric field effect for both w.t. and His85Ala forms of the protein (data not shown) reveal that the mutagenic modification of rusticyanin has not affected the charge symmetry of the protein and corroborates the optical and EPR spectral data that demonstrate retention of Type I copper protein character subsequent to the mutation.

The simplified ESEEM spectrum of His85Ala permits us to examine the behavior of the three principal spectral lines without corruption from either combination lines or possible overlap of lines from two contributing and slightly dissimilar species. The spectrum is immediately recognizable in the context of the interpretation of the copper–imidazole interaction.[17] We do observe a large degree of selection and resolution enhancement of all lines in response to varying the g-value at which the experiment is performed. Alteration of line symmetry and shape of the low-frequency 0.7 MHz component confirms that this low-frequency component of the

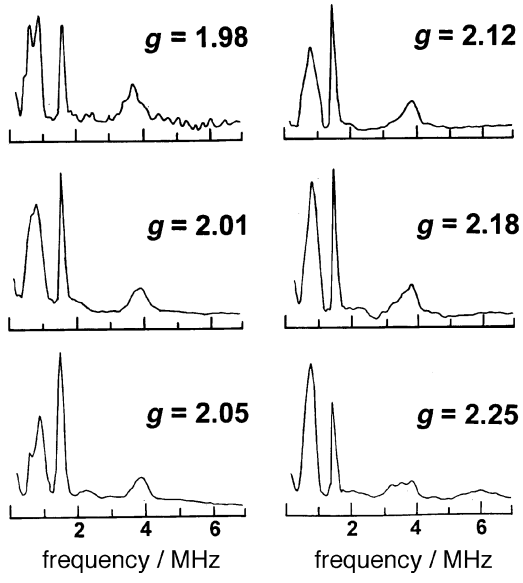

Fig. 5 Stimulated echo modulation spectra of His85Ala rusticyanin, which possesses only a single imidazole ligand to copper, recorded at 9.0 GHz. The data illustrate the g-selection behavior of an ESEEM powder-pattern spectrum for a single weakly coupled ^{14}N. The absence of other components to the classic Mims description substantiates the interpretation of w.t. spectra in the sense that no other interacting nuclei (whose presence may have been masked by the combination lines) contribute to the ESEEM spectrum.

spectrum is indeed an overlap of two lines of width approximately the same as the better resolved 1.5 MHz line. The separation of the two overlapping lines is estimated to be 15–20 kHz, and they do exhibit a measurable magnetic field dependence that is best measured at $g = 1.98$.

Changes in the relative intensity of the 0.7 and 1.5 MHz lines is also indicative of the anisotropy of the quadrupole tensor and that individual components may be 'selected' by recording the ESEEM spectrum at specific g-values. Such selectivity is also observed in the so-called double quantum line at 4 MHz, which changes shape and then resolves into three components at $g \geqslant 2.22$. This apparent broadening of the double quantum line and splitting into three components is surprising because the w.t. $g = 2.25$ spectra (Fig. 2 and 4) do not appear to broaden relative to the $g \approx 2.05$ spectra. The pattern itself, however, can be reproduced by simulations of ESEEM spectra in which the z-axis of the anisotropic quadrupole and hyperfine tensors are nearly orthogonal.

3.6 Relevance of His85Ala spectra to the general interpretation of metal–imidazole ESEEM

The His85Ala ESEEM spectra are significant because they underscore the assigned magnitude of the nuclear quadrupole parameters e^2Qq and η that are inferred from powder metal imidazole ESEEM spectra. The effective zero-field NQR spectrum that is detected in the ESEEM of the weakly coupled imidazole nitrogen can be envisioned as arising from either of two extrema scenarios that differ with respect to the magnitude of η. For example, if η is approximately zero, then the transition $\nu_{10} = \frac{1}{2}e^2Qq\eta$ would likely occur at a frequency that is not detected in the echo modulation time series, and a single-line pattern would be observed. One might argue, therefore, that the typically observed spectral pattern is a superposition of two species of $e^2Qq \approx 1$ MHz and $\eta \leqslant 0.2$, which would yield two fundamental lines (*i.e.* ν_{1+} and ν_{1-}) at *ca.* 0.75 MHz and a harmonic (sum) line at 1.5 MHz. The His85Ala data, however, preclude this interpretation because the now sole $HisN_\varepsilon$ yields exactly the same three-intense-line pattern that is observed for the w.t. ESEEM spectrum.

The second scenario that is consistent with the observed data and now verified by the spectra of the His85Ala mutant protein is that $\eta \approx 1$, which would yield two effective zero-field NQR lines with one approximately half the frequency of the other. This is the implicit interpretation of the preceding sections of this paper and many similar ESEEM studies of copper–imidazole complexes, which was originally derived from the similarity between ESEEM peak positions and the zero-field NQR spectrum of imidazole (see ref. 3, Table 11.16). The two scenarios differ on the strength of the >N—H fragment's hydrogen-bond interactions, which may be appreciated by comparing the gas[37] and solid-state NQR[38] studies of imidazole. When two or more imidazole ligands are present it is impossible to show conclusively that the linewidth at 0.7 MHz is the overlap of two nearby transition frequencies (*i.e.* ν_{10} and ν_{1-}) and not a dispersion of slightly inequivalent ^{14}N nuclei. The resolution of two lines in the 0.7 MHz region of the His85Ala rusticyanin spectrum confirms that the asymmetry factor η is indeed approximately unity.

Very weak features in the 2–3 MHz region of the His85Ala ESEEM spectrum are assigned to $\Delta m_I = 1$ transitions from the m_S spin manifold in which the spin-Hamiltonian terms add. This interpretation is based on their location in the spectrum, which is approximately half the corresponding $\Delta m_I = 2$ transition at 4 MHz. The intensity is very much reduced because the frequencies of these nuclear sublevels in the m_S^+ spin manifold are more dispersed in the powder spectrum and therefore do not modulate the preceding electron spin in any coherent manner. Demonstration that the assignment of the weak 2–3 MHz lines to $\Delta m_I = 1$ transitions is correct and in fact not attributable to other nitrogen atoms coupled to the unpaired electron spin is further corroborated by exploiting the interferogram-like properties of the modulation time series (see below).

Finally, the His85Ala rusticyanin spectrum differs from the ESEEM spectrum of His117Cys azurin, which also features a single histidine imidazole coordinated to copper.[30] In the latter, the two intense low-frequency lines that are ordinarily assigned to the effective zero-field nuclear quadrupole transitions of the remote imidazole nitrogen atom are absent, although they remain in the case of rusticyanin His85Ala. The difference may be attributable to the nature of the His117Cys azurin protein, which does not retain the Type I characteristics unless exogeneous imidazole is added. The His117Cys azurin spectra were recorded with exogenous [^{15}N]imidazole. By contrast, rusticyanin is a very stable protein, and the His85Ala variant retains its Type I characteristics despite a vacancy (H_2O assumes the role of fourth ligand). In fact, the addition of exogeneous imidazole destabilizes the copper binding properties of the His85Ala protein.[29]

3.7 Recovery of information in 'blind spots'

Theoretical expressions of the echo modulation phenomenon reveal that the resultant interferogram depends on the timing parameters that are used in a given experiment.[40,41] The three-pulse echo modulation spectrum will therefore vary as the experiment is repeated with different values of τ,[42] and may be used to aid the assignment of spectral lines in both the w.t. and His85Ala data. This τ-variation in the stimulated echo pulse sequence can be regarded as a quasi-two-dimensional ESEEM experiment, and selective τ manipulation of the echo modulation may be used advantageously to recover information not available in a one-dimensional ESEEM study. A true two-dimensional experiment, however, collected as 256 × 256 time series points, averaged over 100 samples, and at 100 Hz would require over 18 h. A single frequency, multi-τ (*ca.* 6) experiment as described here (1024 points per trace; 100 averages per point) requires 3 h and supplies the requisite deconvolution of spectral lines for interpretation.

Fig. 6 illustrates the echo modulation time series that are

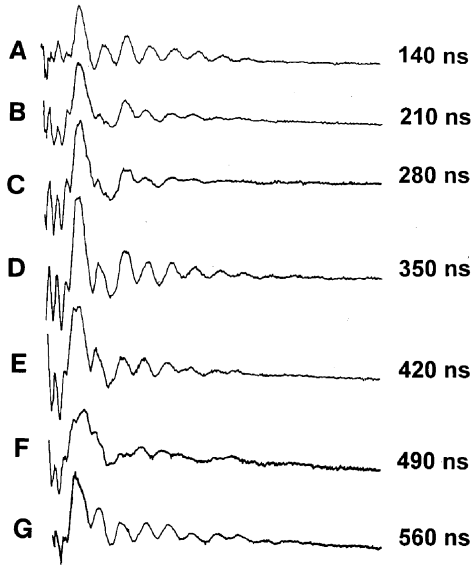

Fig. 6 The effect of varying τ (1–2 interpulse spacing) on the stimulated echo modulation of His85Ala, which demonstrates the 'locking' of a spin precession frequency to the timing of the spin preparation phase of the pulse sequence (see ref. 41 and 42). The deep modulation corresponding to the fundamental (low frequency) are rendered 'transparent' to the detection sequence, exposing weaker modulation.

recorded at several τ values and the resultant suppression of the deep modulation component. The modulation suppressed in the data corresponds to the $\Delta m_I = 2$ transition from the m_S^- spin manifold, and the τ value that best supresses this spectral line corresponds to a multiple of the period of the $\Delta m_I = 2$ transition from the m_S^+ spin manifold. In other words, a τ value that corresponds to a multiple of the period for the 4 MHz double quantum line (*i.e.* $\tau = n\nu_{2+}^{-1}$) will suppress the 1.5 MHz line, the latter of which is the $\Delta m_I = 2$ transition of the opposite m_S spin manifold, ν_{1+}. In general, we can therefore identify the paired $\Delta m_I = 2$ transitions ν_{1+} and ν_{2+} for a specific class of nitrogen atom, and furthermore, when multiple atoms of the same class are present (*e.g.* the w.t. protein with its two $HisN_\varepsilon$), identify the combination and sum lines because they too will be suppressed along with the fundamentals.

The interferogram quality of the echo modulation time series likewise allows us to verify that the very weak features of the His85Ala spectrum are indeed $\Delta m_I = 1$ transitions from the m_S^+ spin manifold. The intensity of the feature at 2 MHz increases as τ is varied through 330 ns (Fig. 7), and a similar effect is observed when τ is further raised to 500 ns, with the enhancement of a 3 MHz line (the 'enhancement' is only in the sense that a masking modulation at 1.5 MHz is removed). All lines can be assigned by comparison to effects demonstrated in Fig. 2 (g-value narrowing and tracking of combination lines), 4 (g-selection of quadrupole lines) and 6 (enhancement of $\Delta m = 1$ transitions).

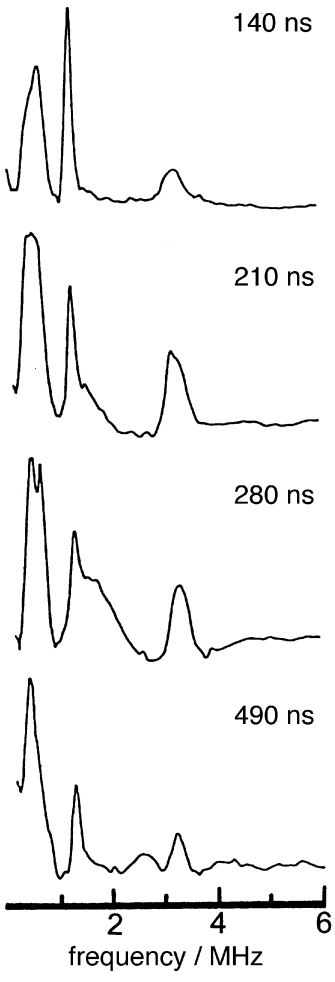

Fig. 7 Select FT spectra from the modulation time series illustrated in Fig. 6. The $\Delta m_I = \pm 1$ transitions from the non-crossing manifold (see text) are now visible as the peaks corresponding to the other spin manifold are suppressed; the suppression technique may be used to identify fundamental lines of the same manifold plus their sums and harmonics, which will respond alike to the spin locking.

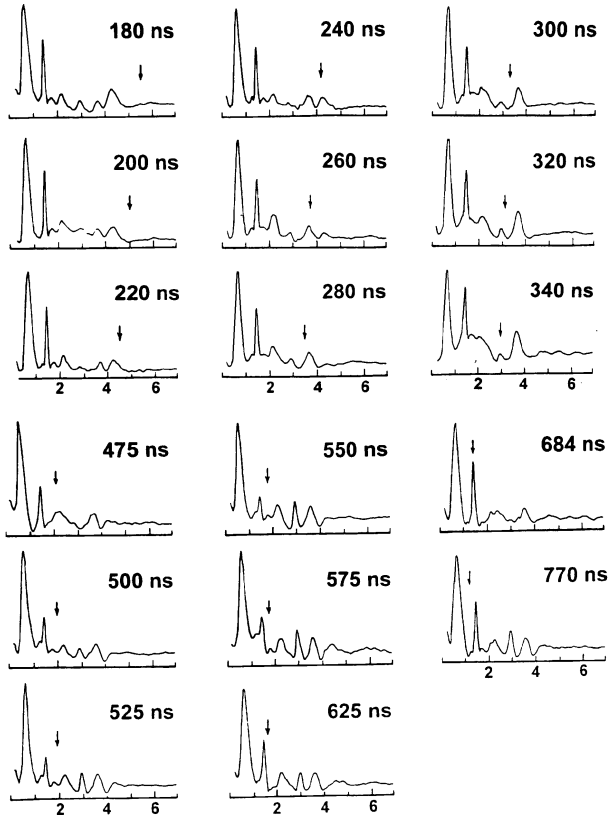

Fig. 8 FT spectra of the select w.t. modulation spectra subjected to the τ suppression effect. The locking frequency (τ^{-1}) is indicated in the spectra by an arrow. This τ-selection enables one to identify and correlate lines by spin manifold origin (see ref. 41), and the Zeeman dependence of the peak position allows one to distinguish a combination line from a $\Delta m_I = \pm 1$ transition or potential fundamental line of a less intense transition frequency.

Finally, Fig. 8 catalogues the more complicated τ dependence of the w.t. protein spectrum and illustrates the effect upon the combination lines when multiple nitrogen couplings contribute to the hyperfine spectrum. The data represent experiments in which τ is incrementally varied so that it becomes approximately the period of a $\Delta m = 2$ transition. Arrows indicate the fundamental frequency corresponding to τ^{-1}, and harmonics (*i.e.* $2\tau^{-1}$ *etc.*) will also be influenced. Repetition of these τ-suppression experiments to attain improved resolution of the weak line across the X-band octave (as illustrated by g-value in Fig. 2) enable careful tracking of peaks for assignment.

4 Refinement of the superhyperfine parameters

4.1 The multifrequency spectrum approach to analysis

The ESEEM spectra of His85Ala indicate that the asymmetry parameter η is very nearly unity because the low frequency feature at *ca.* 0.7 MHz may be resolved as a doublet whose peaks are located approximately 15–20 kHz apart. The simple Townes–Daily formulae for ν_0 and ν_- yield $\eta \approx 0.85$ and $e^2Qq \approx 1.35$ MHz based upon the field dependence data that indicate exact cancellation is near 7.5 GHz. These parametric assignments assume that ν_{10} is the lowest frequency component of the doublet centered near 0.7 MHz (0.55 MHz component in Fig. 3) and ν_{1-} is the higher frequency component (*ca.* 0.88 MHz) of the doublet. Reversal of the assignments yields an absurd value of η (1.3). The resultant parametric values agree well with solid-state NQR data for the >N—H

fragment in free imidazole in the solid state.[3,38] The same experimental data (Fig. 3) indicate that the double quantum transition occurs at 4.3 MHz, from which we estimate that $A_{iso} \approx 1.7$ MHz.

The field dependence of the individual lines attributed to the m_S^- spin manifold and the observation that the same spectral pattern is recorded over more than an octave of microwave operating frequency indicate that the condition of 'exact cancellation' is impossible to specify merely based on the criterion that one observes the classical pattern of two narrow low frequency lines plus the weaker double quantum line. In other words, it is incorrect to assign effective zero-field nuclear quadrupole interaction parameters from a single spectrum. For example, an interpretation based completely on the 9.5 GHz spectrum would lead to a 100 kHz overestimate of e^2Qq. The multifrequency approach that is illustrated in Fig. 2 and yields the representative data listed in Table 1 is therefore necessary to refine the numeric values of the hyperfine parameters. Further simulations of the spectra using the numeric hyperfine parameters as a starting point can then be used to refine the parameters within the limits of a spin-Hamiltonian model and also provide information on the tensor orientations. The details of the simulation 'process' and refinement are outlined in the remainder of this section as a practicum that supplements the original description of the simulation programs.[43]

4.2 Simulations of His85Ala and wild type spectra

The simulation of the copper imidazole ESEEM spectra begins with a starting assumption for the frame of reference (g-tensor) orientation. Single-crystal EPR measurements of azurin[44] and plastocyanin[45] indicate that the g-tensor z-axis is oriented perpendicular to the equatorial plane defined by $CysS_\gamma$ and the two $HisN_\delta$. Assignment of the g_y-axis is arbitrary, but for convenience it is assumed to lie along the $CysS_\gamma$—Cu bond because this axis demarcates an *Ausgewogenheit*[46] plane of symmetry. The ESEEM spectra therefore represent the convolution of hyperfine and quadrupole coupling tensors from two approximately equivalent equatorial nitrogen atoms, and these tensors, at the very least, differ by a rotation about the z-axis of *ca.* 100°, based on the relative positions of the two imidazole rings determined in the crystallographic analysis.

Simulation of the His85Ala, for example, begins with a single nitrogen atom whose nuclear hyperfine and quadrupole tensors are coincident with the g-tensors. Our multifrequency data (see Table 1) indicate that 'exact cancellation is close to 7.5 GHz, and therefore the starting parametric terms are $e^2Qq = 1.4$ MHz, $\eta = 0.85$, and $A_{iso} = 1.7$ MHz. To start, the nuclear hyperfine contribution is considered as being purely isotropic. The dipolar contribution is added later and A_{iso} is adjusted after a best fit is found for the quadrupole tensor because the double quantum line is affected by both Q_{ii} and A_{ii}, whereas we assume that the low-frequency NQI lines are affected by Q_{ii} only. The parameter e^2Qq is signed, but taken as a positive value in these simulations because of the nature of the spin Hamiltonian approximation.

The resultant simulated spectrum at 9.0 GHz features major peaks with assignments $\nu_{10} \approx 0.58$ MHz, $\nu_{1-} \approx 0.87$ MHz, and $\nu_{1+} \approx 1.46$ MHz; the double quantum line, ν_{2+}, appears at *ca.* 4.17 MHz (Fig. 9). Simulations of a single spectrum (*i.e.* field- and τ-value combination) to the level of sophistication illustrated in Fig. 9 are indistinguishable for $0.80 \leqslant \eta \leqslant 0.95$ and $1.40 \leqslant e^2Qq \leqslant 1.60$ MHz, but there is an excellent match to the fundamental frequencies that are experimentally obtained at 9.0 GHz; each of the peaks likewise responds to changes in the Zeeman energy in a manner that mirrors the data trends that were observed by varying the experimental operating frequencies. If the z-axes of the tensors are held coincident in the simulation data, there is no effect of the Euler angle ξ_1.§ Note that the echo decay is modeled by using a Carr–Purcell exponential relaxation with the form $\exp(-t/T_1)^{1/2}$, where T_1 is 2 μs.[47]

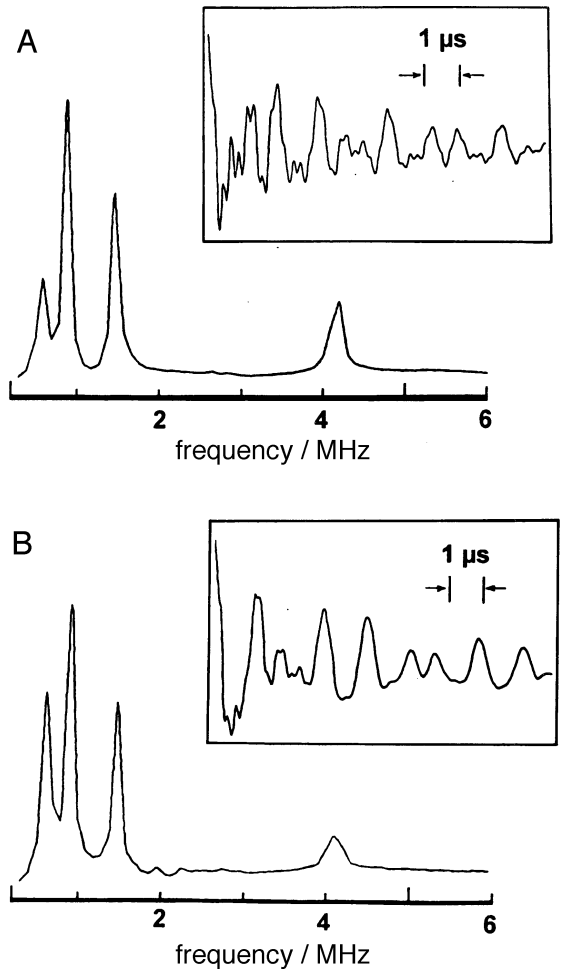

Fig. 9 Simulation of a single weakly coupled ^{14}N ESEEM pattern based on the numerical analysis of the raw data by using the Zeeman dependence of the peak position to refine the estimate. The starting assumption (simulated spectrum A) is that the g-, A-, and Q-tensors are all coincident. The modulation characteristics and FT-spectral characteristics correspond well to the experimental His85Ala data and vindicate the multifrequency graphical procedure for analyzing ESEEM powder patterns. Spectrum B differs from A with respect to the definition of the quadrupole tensor orientation; the z-axis of the quadrupole tensor is perpendicular to g_z in spectrum B. Simulation parameters used: $e^2Qq_{zz} = 1.45$ MHz, $\eta = 0.85$ and $A_{iso} = 1.7$ MHz.

The simulated spectrum that is obtained by using coincident z-axes for all tensors and the hyperfine parameters listed in the preceding paragraph features a ν_{10} transition peak whose intensity is reduced relative to ν_{1-} and ν_{1+}. Because each of the ν_{1i} transitions is weighted differently by q_{zz} and η, the relative intensities of the spectral lines are affected by the the relative orientation of the various tensor axes and therefore may be varied by so-called g-selection, which selects different contributions of the powder pattern hyperfine envelope based on fortuitous alignments (*via* the

§ The generalized notation of A. R. Edmonds, *Angular Momentum in Quantum Mechanics*, Princeton University Press, Princeton, NJ, 1974, is used to specify Euler angles in order to avoid confusion between the otherwise identical M. E. Rose, *Elementary Theory of Angular Momentum*, Wiley, New York, 1957, convention for Euler angles, α, β, γ, and the designations of atoms in hyperfine interaction descriptions. Previous work describing the programs (ref. 42) uses the Rose convention.

selected experimental magnetic field) of tensoral components. This is manifest experimentally as g-dependent peak intensity, which is observed in the experimental spectral line denoted as ν_{10}, whose intensity decreases for $g \leqslant 2.00$ (see Fig. 5). This behavior is therefore used as an aid for refining the relative orientation of the hyperfine and quadrupole tensors. It is noteworthy that the line intensities of the low-frequency components in the w.t. spectra vary more dramatically than the His85Ala spectra (compare Fig. 2 spectra above and below $g = 2.00$), which seems to reflect the orientational inequivalence of the two imidazole side chains in the protein.

The simulations performed with the hyperfine and quadrupole tensors coincident with the molecular reference leave the ν_{10} line intensity too low (relative to ν_{1-} and ν_{1+}), but the requisite intensity is recovered as the Euler angle ξ_2 of the quadrupole tensor, which will be designated ξ_{2Q}, is changed 90°, and its effect is illustrated in Fig. 9B. It is also significant to note that the modulation time series reconstructed with $\xi_{2Q} = 90°$ now lacks the second large oscillatory 'beat' that appears in the first simulation trace (at $t \approx 2$ μs); there is also some damping of the high-frequency double quantum modulation that is more consistent with the experimental data.

The simulated modulation spectra still feature three distinct lines that correspond to the Townes–Daily NQI transition frequencies, but the experimental data do not show such resolution although the spectrometer and associated post-processing numerical methods are capable of distinguishing peaks separated by 20 kHz. The spectral simulations illustrated in Fig. 9 assume that a purely isotropic hyperfine interaction is combined with the nuclear Zeeman energy, that is, these simulated data exclude dipolar interactions and associated dispersion of the spin manifold, which will lead to some broadening of the lines. The program described in ref. 42 for simulating ESEEM spectra computes ENDOR frequencies[48] that are converted to a modulation time series by using the Mims density matrix formalism.[41] Secondly, our field dependence studies of the peak assigned to ν_{1+} suggest that the 7.8 GHz spectrum is above true exact cancellation and $A_{iso} = 1.7$ MHz is actually only an estimate for the nuclear hyperfine interaction. Fig. 10 illustrates the effect of increasing the dipolar contribution to the simulated spectrum: the low frequency NQR peak clearly broadens and seems to shift its maximum towards the experimental center of 0.7 MHz. The modulation likewise seems to 'soften' and lose its depth as the contributing electron–nuclear interaction frequencies become more disperse.

The spectra illustrated in Fig. 10 are generated by using a spin-Hamiltonian model and are aimed at the reproduction of the $g = 2.05$ spectrum in Fig. 5. The spectrum depicted as Fig. 10C is particularly noteworthy because it is a close match to the $g = 2.25$ spectrum in Fig. 5. The tensor orientation parameters that went into simulating Fig. 10C are $g_z \| A_z \perp q_{zz}$, in other words q_{zz} directed along the complex's equatorial plane whereas A_{zz} is perpendicular. Fig. 10C, however, depicts a spectrum that is experimentally observed at only a select g-value (g = 2.25), and because the symmetry of the system is axial, this simulated spectum is identical to one in which $g_z \| q_{zz} \perp A_z$ and is 'observed' at g_z. The similarity between Fig. 5 and 11C, considered in the context of the model system's symmetry and the tensors' Euler angle specifications, indicate that the z-axis of the nuclear hyperfine tensor is very nearly in the equatorial plane of the complex, whereas the z-axis of the quadrupole tensor (taken as the electric field gradient) is directed out of the equatorial plane. The quadrupole tensor is not exactly parallel to g_z because of the relative line intensities of ν_{10}, ν_{1-}, and ν_{1+} are correct only if g_z and q_{zz} are not parallel.

Fig. 11 illustrates the final refinement of simulated spectra at two g-values using the hypothesized tensor orientations; reversing the tensor orientations reverses the g-selection

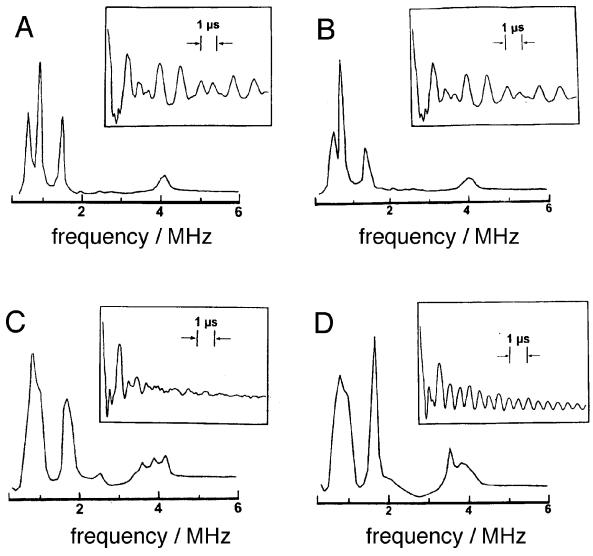

Fig. 10 Refinement of the relative tensor orientation assignment for reproducing the His85Ala ESEEM spectrum. Introducing a dipolar interaction 'corrects' the spectrum in the sense that the ν_{10} and ν_{1-} are broadened and merge, which reproduces the observed lineshape at 0.7 MHz. The simulated peak positions correlate well with *ab initio* calculation estimates of the spin density distribution in a Type I copper site model that are used to estimate the dipolar interaction energy of $HisN_\varepsilon$. The computational model suggests that A_z is very nearly perpendicular to Q_z because the spin density on $HisN_\varepsilon$ is so low. Spectrum A, no dipolar contribution (isotropic A-tensor); spectrum B, 0.25 MHz dipolar interaction; spectrum C, 0.5 MHz dipolar interaction (correct lineshape at 0.7 MHz); D, same as C, but with A_z rendered nearly perpendicular to Q_z, the latter of which forms an acute angle to g_z.

trends. These refined spectral simulations retain non-coincident q_{zz} and g_z axes, and the quality of match between simulation and experiment is good if the angle separating q_{zz} and g_z is *ca.* 35° ($\xi_{2,Q} \approx 35°$). The axis A_z lies along the equatorial plane ($\xi_{2,HF} \approx 90°$), but there is a wide range of acceptable values that will yield an acceptable fit ($\pm 20°$). The tolerances of $\xi_{2,Q}$ are tighter, with acceptable values $35 \leqslant \xi_{2,Q} \leqslant 50°$.

The quantitative analysis of the ^{14}N nuclear quadrupole and hyperfine parameters is possible only by recording the ESEEM spectra at several frequencies. The limitation of analyzing a set of data recorded at a single spectrometer operating frequency was evident by comparing the result of an analysis and simulations made at one frequency to the result of an analysis and simulations performed to match data at several frequencies. An acceptable fit to a single ESEEM spectral set (a set consists of several g-values at a single operating frequency) at 9.0 GHz was obtained by using e^2Qq and η of 1.6 MHz and 0.9; only by repeating the simulations at other operating frequencies and comparing them with the data recorded across the octave is it possible to assign a true numeric parameter. The Zeeman variation and resultant plots of ν_i as a function of the nuclear Zeeman energy are necessary to make accurate determinations of hyperfine parameters, and Table 1 clearly illustrates the Zeeman dependence of the ν_+ transition frequencies. The peak assigned to ν_{2+} (crossing levels, so-called exact cancellation) attains a minimum value that is indicative of the exact cancellation condition and permits a measure of nuclear quadrupole interaction parameters. The experimental data acquired and compiled in the manner suggested in Table 1 are therefore indispensable for quantitative analyses.

The relative orientation of the quadrupole and g-tensors can be used to infer structural information provided that one makes an assumption concerning the relative orientation of

the quadrupole tensor and the atomic coordinates. On the basis of sp^3 orbital hybridization and their presumed role in bonding, the $HisN_\varepsilon$ fragment may be regarded as having C_{3v} symmetry, and by convention one would assign the z-axis to the rotational symmetry axis parallel to the p_z-orbital.[36] Such an assumption would mean that q_{zz} defines the normal to the imidazole ring plane. This would determine the orientation of the nuclear quadrupole electric field gradient, with deviations from this idealized assignment being determined by the effect of the atoms bound to $HisN_\varepsilon$, namely two carbon and one hydrogen atom. The hydrogen atom of the >N—H therefore introduces a possible alternate symmetry axis convention, although the convention of solid- and gas-phase NQR analyses[36] will be assumed.

The same argument applies to the nuclear hyperfine tensor. Ordinarily, the greatest dipole contribution to nitrogen hyperfine is the interaction between the electron in the p_z-orbital and the ^{14}N nucleus. In this case A_{zz} is therefore parallel to the p_z cylindrical axis also. The magnitude of A estimated from the ν_{2+} transition, however, suggests that the spin density on $HisN_\varepsilon$ is very small and the conventional assignment of A_{zz} does not apply. Density functional *ab initio* calculations of the spin density distribution indicate that the dominant terms of the dipolar interaction will stem from the interaction between $HisN_\varepsilon$ and unpaired spin density localized on atomic centers very nearly within the equatorial plane of the complex; simple vector addition of individual A_μ axes suggests that A_{zz} resides in the equatorial plane regardless of the imidazole ring orientation.

On the basis of the arguments outlined in the preceding paragraphs, the single nitrogen simulation data and comparison to the His85Ala (for which there is no X-ray structure) experimental data suggest that the ligand imidazole ring is tilted between 35 and 50° relative to the Cu—$MetS_\delta$ bond; the direction of A_z is not informative. The location and Zeeman dependence of the ESEEM spectral peaks indicate that e^2Qq and η are approximately 1.37 MHz and 0.85, respectively, and the Fermi contact contribution is approximately 1.8 MHz with a dipolar contribution of 0.5 MHz.

These His85Ala data can be assumed as the nuclear quadrupole and hyperfine coupling parameters of the remaining His143, and, to start, used as a fixed quantity for the simulation of w.t. spectra. Fig. 11 likewise illustrates the simulated spectra of the w.t. protein copper site (two ^{14}N electron–nuclear interactions) by using identical quadrupole and hyperfine interaction parameters, and the linewidth constraints upon accurately fitting simulation to experimental data hold the difference between the nuclear quadrupole interaction parameters of the two nitrogen atoms to within 10%. The Euler angles of the tensors of each ^{14}N atomic nucleus are taken at their extrema; in other words, the nuclear quadrupole tensor Euler angles used to represent the two nitrogen atoms are 35 and 50°. This disparity in the tensors does not affect the lineshape of the fundamental lines in any manner that can be used to assign a numeric value to the non-coincidence of the tensors of the two atomic centers. In general, however, the so-called 'combination lines' appear to be informative with regard to relative tensor orientation when the z-axes of the nuclear quadrupole and hyperfine tensors are not coincident with the reference frame. Simulations of spectra reflecting the electron–nuclear interactions of two ^{14}N nuclei indicate that as the quadrupole and hyperfine tensors associated with the two nuclei begin to differ, the combination lines become disperse and lose intensity. Initially, modulation simulations of two nuclei are generated by convolution; identical hyperfine and quadrupole coupling parameters are supplied as program input, but the Euler angle ξ_1, representing the first rotation about the z-axis, differs by *ca.* 100° and represents the different locales of the $HisN_\varepsilon$ relative to the CysS to copper bond. With the tensor z-axes all aligned parallel to g_z, the

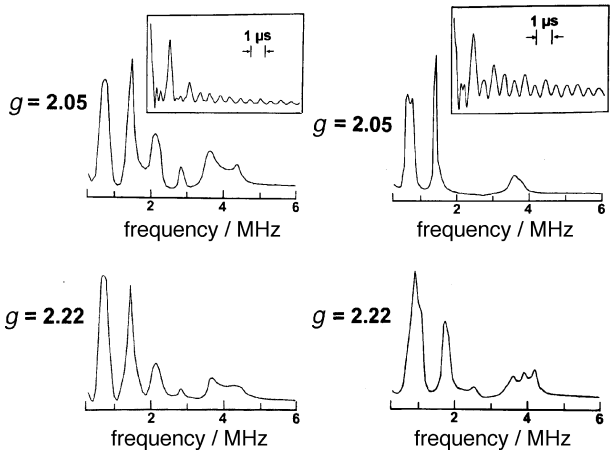

Fig. 11 Final simulations of the w.t. (two nitrogen interactions) and His85Ala (single nitrogen interactions) rusticyanin echo modulation spectra at 9.0 GHz. The match between simulated and experimental spectra is acceptable with the following parameters: $e^2Qq = 1.35 \pm 0.03$ MHz, $0.85 \leqslant \eta \leqslant 0.90$, $A_{iso} = 1.8 \pm 0.1$ MHz, and $A_\mu = 0.5 \pm 0.1$ MHz. The A_z tensor axis is approximately coplanar ($\pm 10°$) with the equatorial ligands, and the quadrupole tensors (two imidazole case) assume a relative orientation of $90 \pm 20°$. Q_z in the single imidazole case is at least tilted off g_z by approximately 35°, with an upper limit of 50°; the single imidazole model jibes with the w.t. fit.

combination lines are sharp and well-defined across the EPR spectral envelope (*i.e.* all g-values). As the second Euler angle ξ_2 (rotation about y′) is varied, the combination lines disperse and seem to have structure, particularly if $\xi_{2A} \neq \xi_{2B}$. The variation among the combination line shapes is observed in ESEEM spectra of *Rhus* and basic blue cucumber stellacyanin; these spectra and the associated simulations illustrating the effect of tensor orientation are to be published separately. As appertains to rusticyanin, however, the match of combination line intensities and breadth between the simulation of the two-nitrogen atom simulation and the w.t. experimental data at $g \approx 2.05$ suggest that the angular disparity of between 75 and 105° is a best case assignment to the difference in ring tilt of the two imidazole ligands to copper in w.t. rusticyanin. The heavy-atom coordinates assigned to the imidazole rings from NMR analysis[13] put this angle at *ca.* 100°.

5 Perturbations to shf interactions

5.1 Anion binding and shifts in the ESEEM spectra of His85Ala

Retention of the Type I copper protein characteristics and exogenous anion binding by His85Ala provide us with a means to determine whether the superhyperfine parameters of $HisN_\varepsilon$ are affected by the nearby equatorial ligand. The rationale for this inquiry comes from the theoretical work of Bertaut, who demonstrated that local charges will influence the electric field gradient of a quadrupolar nucleus.[49] This 'solid-state effect' is routinely observed in the nuclear quadrupole resonance spectra of crystals, but the strong orbital polarization that is characteristic of the Type I copper center[1] and the ability of His85Ala to bind halides as a replacement for the missing histidine made it seem that the His85Ala would be an ideal system in which to test the hypothesis that ESEEM be used as a probe of chemical effects within a metal ion's ligand field.

ESEEM spectra of His85Ala—H_2O, His85Ala—Cl^-, and His85Ala—Br^- are illustrated in Fig. 12, and these data reveal no change in the position of the $\Delta m_I = 2$ transition corresponding to the quadrupole frequency ν_{1+} (the 1.5 MHz

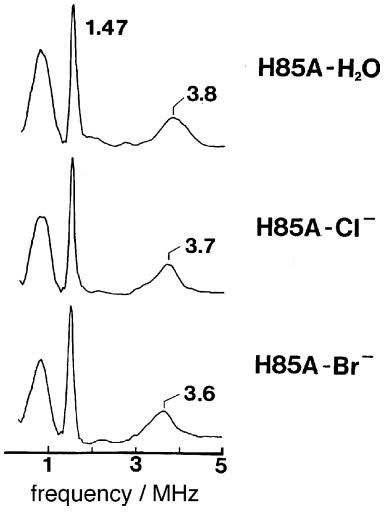

Fig. 12 Perturbation of the His85Ala ESEEM spectrum as the vacancy left by the His85 deletion is filled in succession by H_2O, Cl^- and Br^-. The effective ZF-NQI lines (0.7 and 1.47 MHz) do not appear to shift, suggesting that neither the efg (q_{zz}; orbital hybridization/polarization) and hydrogen bonding interactions (change in η) are affected. The double quantum transition frequency, however, does shift in a fashion that is commensurate with the electron withdrawing power of the substitute ligand, suggesting a change in spin density at the copper atom.

line), although the $\Delta m_I = 1$ lines centered at *ca.* 0.7 MHz seem to have spread apart, as indicated by the apparent line boadening. There is, however, a small measurable shift in the double quantum transition near 4 MHz that, by default, must be attributed to a shift in the spin density distribution defining the electron–nuclear coupling of the remote imidazole nitrogen atom. This downward frequency shift of the double quantum transition increases with the size of the ligand (*i.e.* H_2O, Cl^-, Br^-) and mirrors the changes in intensity of the protein's charge-transfer band; the data suggest that increasing the size of the heavy-atom ligand withdraws unpaired spin density from the remainder of the copper complex (rather than a polarization, solid state effect, that would have been indicated by a shift in ZF–NQI peaks, ν_{1+}, which was not observed).

Evidently, the heavy-atom substitution at the vacancy left by the mutagenic removal of His85 does not affect the NQI parameters of His143N_ε. This came as a disappointment because the precedent NQR spectroscopic studies[50,51] of dichloro- and dibromo-(4*H*-1,2,4-triazole)copper(II) report differences in the amino ^{14}N nuclear quadrupole transition of approximately 20 kHz, which is comparable to the resolution capability of our spectrometer. The fact that we do not observe a shift in the ESEEM spectrum of the protein suggests that the influence of the adjacent ligand upon the remote nitrogen atom of the remaining histidine is smaller than the interaction within the inorganic polymer. One plausible explanation is that NQR spectrum of the copper complex being used as our precedent, which is an inorganic polymer that forms ordered arrays of filaments, is sensitive to halide substitution because the amino nitrogen of the triazole is hydrogen bonded to the halogens of an adjacent filament and this would render the influence of switching halides greater than a simple solid state effect. A second is that the halide is not actually bound as an equatorial ligand to copper in the protein, but nevertheless influences the optical spectrum. We observe no new low-frequency lines that could be interpreted as the halide Larmor line; ENDOR experiments are planned to search for strong couplings indicative of close binding to copper.

5.2 Comparison of experimental data with spin density calculations

Density functional *ab initio* calculations[52] were performed on simple models of the Type I copper motif. The model consisted of CH_3S, CH_3SCH_3, and imidazole fragments that were linked to copper in a fashion that mimicked the Type I copper geometry. Water, chloride, and bromide were sequentially substituted for one imidazole to assess the effect of equatorial ligand exchange on the spin density distribution and electric field gradient at the remote nitrogen atom of the remaining imidazole. In all data reported here, the Becke functional[53] was used.

The data reported here are a portion of a broader study to be published separately, but in summary, the unpaired spin density localized on the imidazole nitrogen atomic centers is low and suggests very little Fermi contact character to nuclear hyperfine. The introduction of higher multiplicity states *via* admixture of low-lying virtual orbitals increases the spin density onto the imidazole ligand, and one obtains the crude electron spin density distribution of 0.25, 0.65, 0.05 (these are magnitudes; the actual data feature a distribution of positive and negative values) for the copper, cysteinyl sulfur and each of the imidazole nitrogens directly coordinated to copper. With water replacing one imidazole ligand, the spin density on copper was $\rho_{Cu} = 0.26$, thiol sulfur $\rho_S = 0.71$, imidazole (coordinated) nitrogen $\rho_{N\delta} \approx 10^{-2}$, and oxygen (water) $\rho_O = 0.01$. Computational models of halide binding yielded shifts of electron spin density. A model of His85Ala—Cl^- featured a copper spin density of $\rho_{Cu} = 0.20$, a thiol sulfur spin density of $\rho_S = 0.55$, an imidazole (coordinated) nitrogen spin density of $\rho_{N\delta} \approx 10^{-3}$, and a chloride spin density of $\rho_{Cl} = 0.26$. Density functional calculations with a His85Ala—Br model further reduced the unpaired spin density associated with the copper ($\rho_{Cu} = 0.15$), whereas the spin density of the thiol sulfur and N_δ of the remaining imidazole did not further change by any significant amount. Likewise, the spin density localized on the bromine atomic center is only slightly larger than the corresponding chloride. These results concur with the experimental data which suggests that the electron spin density, as represented by the magnitude of the ^{14}N nuclear hyperfine interaction and frequency of the double quantum line, is being withdrawn from copper by the halide ion. The fact that the copper spin density only seems to be affected implies that the observed shift of the double quantum line reflects a change in the dipolar interaction between $HisN_\varepsilon$ and the unpaired spin density on copper[54]. These data also seem to suggest that the nature of the nuclear hyperfine tensor is predominantly dipolar because, despite the predicted withdrawal of substantial spin density from the Cu—N 'bond', the ESEEM spectrum of the remote nitrogen is only slightly affected.

The ESEEM and *ab initio* spin densities of the His85Ala variants make for an interesting result that may help assign the nuclear hyperfine tensor orientation. Often it is stated that the *z*-axis is directed perpendicular to the plane defined by the atomic coordinates of the >N—H fragment, but this is based on EPR studies of tricoordinate nitrogen for which there is a significant spin density associated with the nitrogen p_z-orbital. When the self-dipole interaction dominates, the *z*-axis clearly lies along the axial symmetry axis of the p_z-orbital. The *ab initio* calculations indicate that there is very little spin density on $HisN_\varepsilon$, which suggests that dipolar terms are all approximately equal and that, using vector addition, A_{zz} may very likely not be normal to the imidazole plane. The ρ_{Cu}–nitrogen dipolar interaction might, for example, dominate the nuclear hyperfine tensor. It therefore follows that if the equatorial ligand substitution only significantly affects ρ_{Cu} it would still affect the double quantum transition frequency, and the scaling factor would be the Cu—$HisN_\varepsilon$ distance. In summary, the *ab initio* data suggest that there is no alteration of the

$HisN_\varepsilon$ spin density of efg, but does affect the spin density on Cu and CysS. Our experimental data indicate that only the double quantum line is affected, which concurs with the *ab initio* data and suggests the ρ_{Cu}–$HisN_\varepsilon$ dipolar interaction dominates. This, in turn, suggests that A_{zz} lies along, but not parallel to (see ref. 53), the Cu—$HisN_\varepsilon$ vector.

6 Conclusion

6.1 General conclusions from the analytic procedure

Our aims in conducting this ESEEM study of rusticyanin and its His85Ala variant have been manifold. We have demonstrated that the superhyperfine parameters of quadrupolar nuclei can be numerically assigned to a high degree of accuracy from powder patterns through the application of a systematic multifrequency experimental protocol.[18] The His85Ala ESEEM data have also clearly demonstrated that weak superhyperfine interactions, such as those of the type $-CH_2S\cdots H-N<$ or amino groups within the ligand sphere, are not responsible for ESEEM spectral features in the 2–4 MHz region. The multifrequency data furthermore demonstrate that the peaks that do appear in the this region of the w.t. ESEEM spectrum obey a Zeeman dependence to peak position that mirrors the Zeeman dependence of the intense effective zero-field NQI lines. We propose that this multifrequency approach to the examination of Zeeman dependent behavior of weak ESEEM lines is an accurate way to identify and assign these lines. The fundamental 'exact cancellation' NQI lines and their so-called combination lines will move in tandem and trace out a parabolic pattern when plotted as peak position *vs.* Zeeman energy. Other peaks that arise from transitions not subject to exact cancellation will not follow a parabolic trajectory and may be distinguished on this basis.

A second means of distinguishing combination lines from fundamental lines associated with other weakly coupled nuclei, such as peptide amino groups, has been demonstrated by exploiting the Mims density matrix formalism and its identificaton of 'blind spots' according to simple rules. Tau suppression by effectively spin-locking the pulse excitation sequence to a specific precession (*i.e.* transition) frequency enables one to identify the partner transition in the other spin manifold. The combination lines collapse along with their fundamentals and thereby provide a means of peak identification. Our studies also indicate that the normally masked $\Delta m = 1$ transitions of the non-crossing spin manifold may be recovered. In summary, therefore, our in-depth examination of the Zeeman field and *g*-selection dependence of ESEEM spectra of a well characterized biological metal complex has enabled us to set forth a reliable experimental protocol for culling superhyperfine parameters from a powder ESEEM spectrum.

6.2 Application of ESEEM to molecular design

A second aspect of this study concerns a test as to whether powder ESEEM spectra and their current analytic state-of-the-art may be used in a quantitative manner to study chemical effects. Substitution of ions at the site of a vacancy in a metal ions ligand sphere by using an engineered protein has yielded spectra whose peaks shift in a manner that concurs with chemical expectations (seen as an apparent decrease of spin density from the copper–imidazole interaction). The double quantum line of $His143N_\varepsilon$ shifts to lower frequency as the electron-withdrawing properties of the exogenous ligand increases; these data concur with chemical principles of hyperfine interactions and *ab initio* calculations based on Type I copper site models. A polarization, or solid state, effect was not detected, which would have been manifest as a shift in the ZF-NQI peaks.

6.3 The superhyperfine parameters of rusticyanin

Finally, our data and its comparision with spectral simulations suggest that the quadrupole parameters of both $HisN_\varepsilon$ are similar; $e^2Qq = 1.37 \pm 0.03$, and $0.85 \leqslant \eta \leqslant 0.90$. The nuclear hyperfine tensor parameters are less precisely obtained because of dipolar broadening and furthermore seem to vary more among the two forms of the protein. A good fit of simulated to experimental spectra across the X-band octave is achieved with an isotropic hyperfine contribution of 1.8 MHz and a dipolar interaction energy of 0.5 MHz. Our analysis of simulated lineshape as a function of tensoral orientation indicates that the quadrupole and hyperfine tensor are not coincident and their *z*-axes differ by a minimal angle of 60°, with A_z nearly coplanar with the equatorial plane. The analysis of the His85Ala ESEEM spectra suggest that the quadrupole tensor of $His143N_\varepsilon$ are tilted off the g_z reference axis by approximately 40°, and the w.t. spectrum analysis indicates that the two HisN reference frames differ by 90 ± 15°, which concurs with the NMR structure.

Our experimentally determined numerical values for quadrupole parameters e^2Qq and η (0.85) differ from the free imidazole values in the gas phase ($e^2Qq_{zz} = -2.54$; $\eta = 0.29$[37]), but are similar to the resultant data of condensed phase NQR spectra ($e^2Qq_{zz} = -1.425$; $\eta = 0.98$[38]). The values of e^2Qq for the protein and imidazole in condensed phase agree to within the confidence level of the powder ESEEM spectroscopic method (spectral simulations rule out the quadrupole parameters of the gas phase molecule). The lower value of η for the protein sample, however, differs from the NQR value by an amount greater that the error bounds of our analysis and suggests that there is a lesser tendency of the $HisN_\varepsilon$ hydrogen to interact with its surroundings *via* hydrogen bonding interactions (as compared to the presumably $>N-H\cdots N<$ interaction of solid imidazole). No appreciable difference in the quality of fit between simulated and experimental ESEEM spectra were obtained if a sign convention (*i.e.* −1.37 MHz) was used for the e^2Qq input parameter. It is also noteworthy that by using the analytical techniques described in this paper, we find that the e^2Qq of $HisN_\varepsilon$ in rusticyanin is approximately 100 kHz smaller than that of stellacyanin.[55]

The comparison of ESEEM spectra obtained from w.t. and His85Ala forms of the protein is relevant to protein engineering. The improved spectral resolution of ESEEM (and presumably ENDOR) have enabled us with the ability to assess at least one side chain interaction in the vicinity of the copper binding site; the close similarity between the $HisN_\varepsilon$ nuclear quadrupole coupling parameters suggests that hydrogen bonding interactions between this imidazole nitrogen and the adjacent amino acid chain is not affected. This, together with the identical LEFE profiles of the w.t. and mutant forms of the protein indicate that the copper site is not measurably perturbed by the substitution of His85 by alanine. This is not true of the azurin from *Pseudomonas.*

This research was supported by the National Institutes of Health, contracts RR-02583 (J.P., C.J.B.) and GM48374 (H.J.D.). *Ab initio* calculations were conducted at Emory University's Emerson Center for Theoretical Chemistry, to which C.J.B. is grateful for an Emerson Fellowship during the 1995 academic year.

References

1 E. I. Solomon, M. J. Baldwin and M. D. Lowery, *Chem. Rev.*, 1992, **92**, 521.
2 J. C. Cox and D. H. Boxer, *Biochem. J.*, 1978, **174**, 497.
3 E. A. C. Lucken, *Nuclear Quadrupole Coupling Constants*, Academic Press, London, 1969.
4 E. T. Adman, *Adv. Protein Chem.*, 1991, **42**, 145.
5 M. Ronk, J. E. Shively, E. A. Shute and R. C. Blake, *Biochemistry*, 1991, **30**, 9435.

6 T. Yano, Y. Fukumori and T. Yamanaka, *FEBS Lett*., 1991, **288**, 159.
7 F. Nunzi, M. Woodstra, D. Campese, J. Bonicel, D. Morin and M. Bruschi, *Biochim. Biophys. Acta*, 1993, **1162**, 28.
8 S. D. Holt, B. Piggott, W. J. Ingledew, M. C. Feiters and G. P. Diakun, *FEBS Lett*., 1990, **269**, 117.
9 J. G. Grossman, W. J. Ingledew, I. Harvey, R. W. Strange and S. S. Hasnain, *Biochemistry*, 1995, **34**, 8406.
10 A. H. Hunt, A. Toy-Palmer, N. Assa-Munt, J. Cavanagh, R. C. Blake II and H. J. Dyson, *J. Mol. Biol*., 1994, **244**, 370.
11 D. R. Casimiro, A. Toy-Palmer, R. C. Blake II and H. J. Dyson, *Biochemistry*, 1995, **34**, 6640.
12 A. Toy-Palmer, S. Prytulla and H. J. Dyson, *FEBS Lett*., 1995, **365**, 35.
13 M. V. Botuyan, A. Toy-Palmer, J. Chung, R. C. Blake II, P. Beroza, D. A. Case and H. J. Dyson, *J. Mol. Biol*., 1996, **263**, 752.
14 R. L. Walter, S. E. Ealick, A. M. Friedman, R. C. Blake II, P. Proctor and M. Shoham, *J. Mol. Biol*., 1996, **263**, 730.
15 S. A. Dikanov and Yu. D. Tsvetkov, *Electron Spin Echo Envelope Modulation* (*ESEEM*) *Spectroscopy*, CRC Press, Boca Raton, FL, 1992.
16 E. L. Hahn, *Phys. Rev*., 1950, **50**, 580.
17 W. B. Mims and J. Peisach, *J. Chem. Phys*., 1978, **69**, 4921.
18 D. J. Singel, in *Advanced EPR: Applications in Biology and Biochemistry*, ed. A. J. Hoff, Elsevier, Amsterdam, 1989, p. 119.
19 J.-M. Fauth, A. Schweiger, L. Braunschweiler, J. Forrer and R. R. Ernst, *J. Magn. Reson*., 1986, **66**, 74.
20 D. M. S. Bagguley, in *Pulsed Magnetic Resonance: NMR, ESR, and Optics*, ed. D. M. S. Bagguley, Clarendon Press, Oxford, 1992, p. 1.
21 W. B. Mims, *Rev. Sci. Instrum*., 1974, **45**, 1583.
22 W. B. Mims, *J. Magn. Reson*., 1984, **59**, 291.
23 A. A. Shubin and S. A. Dikanov, *J. Magn. Reson*., 1983, **52**, 1.
24 H. L. Flanagan and D. J. Singel, *J. Chem. Phys*., 1987, **87**, 5606.
25 M. Iwasaki, K. Toriyama and K. Nunome, *J. Chem. Phys*., 1987, **86**, 5971.
26 E. M. Corson, *Perturbation Methods in the Quantum Mechanics of n-Electron Systems*, Blackie, London, 1951.
27 C. H. Townes and A. L Schalow, *Microwave Spectroscopy*, McGraw-Hill, New York, 1955.
28 D. Kosman, J. Peisach and W. B. Mims, *Biochemistry*, 1980, **19**, 1304.
29 R. S. Carson, *Radio Communication Concepts: Analog*, Wiley, New York, 1990, ch. 1.
30 J. W. A. Coremans, M. van Gastel, O. G. Poluektov, E. J. J. Groenen, T. den Blaauwen, G. van Pouderoyen and G. W. Canters, *Chem. Phys. Lett*., 1995, **235**, 202.
31 E. N. Baker, *J. Mol. Biol*., 1988, **203**, 1071.
32 R. Cammack, A. Chapman, J. McCracken, J. B. Cornelius, J. Peisach and J. H. Weiner, *Biochim. Biophys. Acta*, 1988, **956**, 307.
33 M. van de Kamp, G. W. Canters, S. S. Wijmenga, A. Lommen, C. W. Hilbers, H. Nar, A. Messerschmidt and R. Huber, *Biochemistry*, 1992, **31**, 10194.
34 J. E. Roberts, T. G. Brown, B. M. Hoffman and J. Peisach, *J. Am. Chem. Soc*., 1980, **102**, 825.
35 M. M. Werst, C. E. Davoust and B. M. Hoffman, *J. Am. Chem. Soc*., 1991, **113**, 1533.
36 L. Kevan and L. D. Kispert, *Electron Spin Double Resonance Spectroscopy*, Wiley, New York, 1974.
37 D. Christen, J. H. Griffiths and J. Sheridan, *Z. Naturforsch*., *Teil A*, 1982, **37**, 1378.
38 M. J. Hunt, A. L. Mackay and D. T. Edmonds, *Chem. Phys. Lett*., 1975, **34**, 473.
39 D. R. Casimero and H. J. Dyson, unpublished results.
40 L. G. Rowan, E. L. Hahn and W. B. Mims, *Phys. Rev. A*, 1965, **137**, 61.
41 W. B. Mims, *Phys. Rev*., 1972, **5**, 2409.
42 R. P. J. Mercks and R. deBeer, *J. Phys. Chem*., 1979, **83**, 3319.
43 J. B. Cornelius, J. McCracken, R. B. Clarkson, R. L. Belford and J. Peisach, *J. Phys. Chem*., 1990, **94**, 6977.
44 J. W. A. Coremans, O. G. Poluektov, E. J. J. Groenen, G. W. Canters, H. Nar and A. Messerschmidt, *J. Am. Chem. Soc*., 1994, **116**, 3097.
45 K. W. Penfield, R. R. Gay, R. S. Himmelwright, N. C. Eickman, V. A. Norris and H. C. Freeman, *J. Am. Chem. Soc*., 1981, **103**, 4382.
46 H. Weyl, *Symmetry*, Princeton University Press, Princeton, NJ, 1952. p. 16.
47 J. R. Klauder and P. W. Anderson, *Phys. Rev*., 1962, **125**, 912 (eqn. 2.16 and 5.1).
48 G. C. Hurst, T. A. Henderson and R. W. Kreilick, *J. Am. Chem. Soc*., 1985, **107**, 7294.
49 E. F. Bertaut, *J. Phys. Rad*., 1952, **13**, 499.
50 T. Asaji, H. Sakai and D. Nakamura, *Inorg. Chem*., 1983, **22**, 202.
51 T. Asaji, J. Ishikawa, R. Ikeda, M. Inoue and D. Nakamura, *J. Magn. Reson*., 1981, **44**, 126.
52 M. J. Frisch, G. W. Trucke, H. B. Schlegel, P. M. W. Gill, B. G. Johnson, M. A. Robb, J. R. Cheeseman, T. Keith, G. A. Petersson, J. A. Montgomery, K. Raghavachari, M. A. Al-Laham, V. G. Zakrzewski, J. V. Ortiz, J. B. Foresman, J. Ciolowski, B. B. Stefanov, A. Nanayakkara, M. Challacombe, C. Y. Peng, P. Y. Ayala, W. Chen, M. W. Wong, J. L. Andres, E. S. Replogle, R. Gomperts, R. L. Martin, D. J. Fox, J. S. Binkley, D. J. Defrees, J. Baker, J. P. Stewart, M. Head-Gordon, C. Gonzalez and J. A. Pople, GAUSSIAN 94, Revision D.3; Gaussian, Inc., Pittsburgh, PA, 1995.
53 A. D. Becke, *Phys. Rev. A*, 1988, **38**, 3089.
54 B. A. Goodman and J. B. Raynor, *Adv. Inorg. Chem. Radiochem*., 1970, **13**, 136.
55 C. J. Bender, unpublished results.

Paper 7/04541G; *Received* 27*th June*, 1997